

# **Design of Polarization Splitter and Rotator**

*A THESIS*

*submitted by*

**SIREESHA NAMBIGARI R**  
**EE09B056**

*in partial fulfilment of the requirements*  
*for the award of the degree of*

**BACHELOR AND MASTER OF TECHNOLOGY**



**DEPARTMENT OF ELECTRICAL ENGINEERING**  
**INDIAN INSTITUTE OF TECHNOLOGY MADRAS.**

**May 2014**

# THESIS CERTIFICATE

This is to certify that the thesis titled **Design of Polarization Splitter and Rotator**, submitted by **Sireesha Nambigari R**, to the Indian Institute of Technology, Madras, for the award of the degree of **B.Tech and M.Tech (Dual Degree)**, is a bona fide record of the research work done by her under my supervision. The contents of this thesis, in full or in parts, have not been submitted to any other Institute or University for the award of any degree or diploma.

**Dr. Bijoy Krishna Das**  
Research Guide  
Associate Professor  
Dept. of Electrical Engineering  
IIT-Madras, 600 036

Place: Chennai

Date: 6th May 2014

## **ACKNOWLEDGEMENTS**

Acknowledgement is redundant as no amount of words can express the gratitude you have towards those who helped you. However I would like to take this opportunity to thank my guide Dr. Bijoy Krishna Das for shaping up my interest in the field of silicon photonics through all the courses I have taken under him and for being a continuous source of encouragement.

I would also like to thank Dr Nandita Dasguta for being the most awesomest faculty advisor ever. However big or small the problem maybe, she was always there to help me sort it out. My friends Shravani, Mounika, Niharika and Keerthi have always been there for me, with me, through good and through bad. A big thanks to all my batchmates who made insti a fun place to be in, adding loads of laughter to it, each day, making it all the more difficult for me to leave this place.

A special thanks to my mentor Sidharth, my active acting mentor Meenatchi and my proactive mentor Saket, for all their time and energy spent on familiarizing me with my DDP. I would also like to thank my friends Riddhi, Vivek, Sumi, Rashmi, Sujith, Dada, Parimal, Varun, Shantanu, Mandar and Sreevatsa for being so approachable regarding any queries that I had and for making my final year in insti memorable.

It goes without saying, I bow to my family for giving me the freedom of choice, that made me what I am today.

# ABSTRACT

Due to its small geometrical structures and compatibility with CMOS technology, the silicon photonic wire waveguide provides us a unique platform of integrated optoelectronic devices. However, ways must be figured out to reduce the propagation loss, coupling loss to external fibers and overcome the polarization dependence. Polarization dependence remains a serious obstacle to the practical applications of these waveguides.

In the work presented, the design of a polarization splitter and rotator (PSR) is improved and made fabrication tolerant. Alternate structures and design parameters for the PSR are discussed. The PSR structure is formed by joining an adiabatic taper with a Y junction and MMI coupler. Alternate designs that can be used instead of extra path length for achieving a 90 degree phase difference are discussed. A 2x2 MMI is optimized to achieve maximum efficiency. All the simulations for the optimization of the design are done using the Lumerical FDTD simulation tool. The output of the polarization splitter and rotator will always be  $TE$  polarized which is independent of input polarization state ( $TE$  or  $TM$ ). This PSR structure is simulated for SOI platform with silicon thickness being 250 nm and buried  $SiO_2$  being 3  $\mu\text{m}$ . The total device length is around 230  $\mu\text{m}$ . The output efficiency of this device for  $TE$  input state is 96.3 percent and for  $TM$  input state it is 100 percent.

# TABLE OF CONTENTS

<b>ACKNOWLEDGEMENTS</b>	<b>i</b>
<b>ABSTRACT</b>	<b>ii</b>
<b>LIST OF FIGURES</b>	<b>vi</b>
<b>1 Introduction</b>	<b>1</b>
1.1 Background . . . . .	1
1.2 Guided modes and birefringence . . . . .	2
1.3 Polarization Diversity circuits . . . . .	3
1.4 Research Objective . . . . .	6
1.5 Thesis Organization . . . . .	7
<b>2 Allowed modes in a SOI waveguide</b>	<b>8</b>
2.1 Single mode condition . . . . .	8
2.2 $TM_0$ - $TE_1$ hybridization . . . . .	12
2.3 Design of an adiabatic taper structure . . . . .	12
<b>3 Design of polarization splitter and rotator</b>	<b>15</b>
3.1 Design of Y - Splitter . . . . .	15
3.2 Combining the adiabatic taper and the Y - splitter . . . . .	17
3.3 MMI Design . . . . .	18
3.4 90 degree Phase shift . . . . .	21
3.5 Principle and working of the PSR . . . . .	23
3.6 Tolerance analysis of Y - Splitter . . . . .	24
3.7 Complete structure . . . . .	26
<b>4 Summary and future work</b>	<b>27</b>
4.1 Summary . . . . .	27
4.2 Future work . . . . .	27

## LIST OF TABLES

2.1	Exclusive single moded waveguides . . . . .	9
2.2	Waveguide dimensions that allow 3 modes . . . . .	10
2.3	Waveguide dimensions that allow upto 4 modes with completely evolved $TE_1$ mode . . . . .	11
3.1	Variation of efficiency with Y-spiltter gap. . . . .	25

## LIST OF FIGURES

1.1	Structure of a Photonic wire waveguide . . . . .	2
1.2	Stress induced by the top cladding . . . . .	4
1.3	A Polarization Diversity Circuit [6] . . . . .	5
1.4	Block diagram representation of a PSR . . . . .	5
2.1	Effective Index for different modes as a function of varying width where the blue circle shows the critical point that allows mode conversion between $TM_0$ and $TE_1$ . . . . .	12
2.2	Detailed schematic of the taper section with design parameters . . .	13
2.3	FDTD simulated $E_y$ profile of the light wave when $TE_0$ is launched	13
2.4	FDTD simulated magnitude profile of the light wave when $TM_0$ is launched . . . . .	14
2.5	(a) FDTD simulated magnitude profile of the output mode at the end of the taper when $TE_0$ is launched, (b) FDTD simulated $E_y$ profile of the output mode at the end of the taper when $TM_0$ . . . . .	14
3.1	Detailed schematic of the Y-Splitter with design parameters . . . . .	15
3.2	FDTD simulated $E_y$ profile of the light wave when $TE_0$ is launched	16
3.3	FDTD simulated $E_y$ profile of the light wave when $TE_1$ is launched	16
3.4	(a) Simulated $E_y$ mode profile of the light wave at the end of the splitter, when $TE_0$ , (b) Simulated $E_y$ mode profile of the light wave at the end of the splitter, when or $TM_0$ is launched . . . . .	17
3.5	Simulated $E_y$ profile of the light wave when $TE_0$ is launched . . . .	17
3.6	Simulated magnitude profile of the light wave when $TM_0$ is launched	17
3.7	3D view of the PSR structure . . . . .	18
3.8	(a) Simulation of a $3\ \mu\text{m}$ width MMI structure with 0 degree phase difference between the two sources, (b) Simulation of a $3\ \mu\text{m}$ width MMI structure with 90 degree phase difference between the two sources .	19
3.9	(a) Simulation of a $4.2\ \mu\text{m}$ width MMI structure with 0 degree phase difference between the two sources, (b) Simulation of a $4.2\ \mu\text{m}$ width MMI structure with 90 degree phase difference between the two sources	20
3.10	MMI design parameters . . . . .	21
3.11	Schematic of the 90 degree phase difference using width variation .	21

3.12	Simulated structure of device using width variation for 90 degree phase difference . . . . .	22
3.13	Schematic of the 90 degree phase difference using taper length variation	22
3.14	Simulated structure of device using taper length variation for 90 degree phase difference . . . . .	23
3.15	Topview of PSR with all the components . . . . .	24
3.16	Y - splitter with a gap of 100nm . . . . .	25
3.17	Simulation of the complete PSR structure when $TM_0$ is launched . .	26
3.18	Simulation of the complete PSR structure when $TE_0$ is launched . .	26



# CHAPTER 1

## Introduction

### 1.1 Background

As the geometries of VLSI chips become smaller and denser, and as computations become faster and more complex, the capacity of electric circuits is being outstripped. The connections simply cannot handle electric signals fast enough and process them. Exploiting the fact that light travels faster than electronic signals, we can connect circuits by light as a medium for data flow instead of electrical signals. Optical interconnects offer an excellent alternative in the form of on-chip waveguide, with the added advantage of higher bandwidth and lower power dissipation. Due to its transparency in the range of optical wavelengths, silicon can be used for making these optical interconnects which offer smaller delay and better resistance to electromagnetic interference than conventional electronic interconnects [1].

Silicon photonics, the emerging technology is associated with signal generation, processing, transmission and detection where the signal is carried by light in silicon-based components. Perhaps the greatest benefit of Silicon photonics is the cost effectiveness, in addition to the performance gain via integrating different types of optical devices onto a single silicon platform together with the already existing integrated electronics.

Waveguides are the most fundamental component for all of the silicon photonic devices. These devices, work on Silicon-on-insulator (SOI) platform [2]. The silicon layer is sandwiched between the buried insulator and top cladding of air. As the refractive indices of these claddings are lower than that of silicon, propagation of electromagnetic waves in the waveguides is possible on the basis of total internal reflection.

In a typical waveguide (see Fig 1.1), light is confined in two directions, in both x and y direction and is guided along the propagation direction z. Pure TE and TM modes do not exist in these waveguides, instead we have hybrid modes called TE like modes ( $E_x$  and  $H_y$  dominate) and TM like modes ( $E_y$  and  $H_x$  dominate).

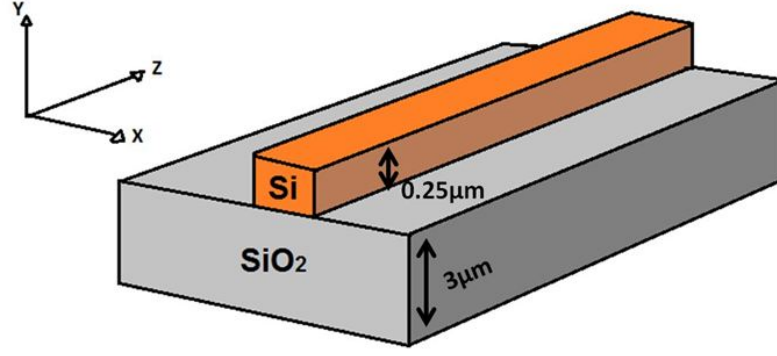


Figure 1.1: Structure of a Photonic wire waveguide

Photonic wire waveguides can confine light strongly due to the large refractive-index difference between Si and  $SiO_2$  ( $\Delta n = 2$ ). This difference in refractive index allows us to make core sizes in the order of submicron dimensions, which can provide single-mode propagation at a wavelength of  $1.55 \mu\text{m}$ . Moreover, strong confinement allows sharp bends (loss with strong confinement is low) with radii of just a couple of micrometers [3]. Therefore, Si wire waveguides enable us to make optical circuits that are compact in size.

## 1.2 Guided modes and birefringence

Polarization is a property of electromagnetic waves that describes the orientation of the electric and magnetic field oscillations. A lightwave of arbitrary polarization can be represented as the linear superposition of two orthogonally polarized modes, Transverse electric ( $TE$ , electric field parallel to the wafer plane in a planar waveguide) and Transverse magnetic ( $TM$ ) modes. Polarization dependent losses in silicon waveguides is mainly due to scattering from the waveguide core-cladding interfaces.

As light is composed of both electrical and magnetic components, the velocity of light through a substance is partially dependent upon the electrical conductivity of the material. The relative speed at which electric signals travel through the material varies with the type of signal and its interaction with the structure, and is determined by the dielectric constant of that material. Dielectric constant intern depends on refractive index of the material as  $\epsilon = n^2$

Waveguide birefringence is defined as the difference between the effective indices

of polarized  $TE$  mode and polarized  $TM$  mode. The electric field distributions of the  $TE$  and  $TM$  modes satisfy the boundary conditions at the interface between two different material layers. When surface electric charge and current density are absent, the tangential field components and the normal components of the electric displacement  $D = \epsilon E$  and the magnetic induction  $B = \mu H$  are continuous across the boundary interface. The high index contrast of the core and cladding layer on a SOI platform presents a large discontinuity in  $\epsilon$  at the interface layer for the propagating light. [4].

$$E_{1t} = E_{2t}, H_{1t} = H_{2t} \text{ (Tangential)}$$

$$D_{1n} = D_{2n}, B_{1n} = B_{2n} \text{ (Normal)}$$

The propagating light must satisfy the boundary conditions imposed by the waveguide (symmetric in x direction with air on both sides and assymmetric in y direction with air on top and  $SiO_2$  on the bottom). Thus  $TE$  and  $TM$  properties are no longer the same, leading to a non-zero birefringence. Birefringence in SOI waveguides is governed by the waveguide cross-section and stress in the silicon core.

When light travels in a dielectric waveguide, the phase velocity  $v$  is reduced to  $v = \frac{c}{n_{eff}}$ , where  $n_{eff}$  is the effective index of the waveguide and  $c$  is the speed of light in free space. Waveguide birefringence describes the anisotropy with respect to polarization in the propagation constant (or the effective index) of the optical modes. Light waves with different polarization states travel at different speeds when a waveguide is birefringent. In such waveguides [5], the electric and magnetic oscillations are no longer perpendicular to the direction of travel, but have an appreciable amount of field component in the direction of propagation.

Polarization dependence of waveguides presents one of the most difficult challenges in the design of planar waveguide components.

### 1.3 Polarization Diversity circuits

Silicon waveguide that have large structural birefringence causes polarization mode dispersion and polarization dependent loss [6]. Some optoelectronic devices like ring resonators [7], raman lasers [8], filters [9] are optimized for a single polarization either  $TE$  or  $TM$ . Therefore, polarization dependence remains a serious obstacle to the efficient functioning of these circuits [10]. To make a photonic circuit polarization

independent, the simplest way is to use a square core waveguide (same cladding surrounding the core). Owing to the fact that a silicon waveguide has a high-index-contrast, fabrication errors of just a couple of nanometers are critical and result in birefringence.

Another way of eliminating polarization dependence is stress [11] engineering(see Fig 1.2). Stress distribution in a waveguide depends on the core and cladding material constants and the waveguide geometry. This stress causes the material refractive indices to change accordingly [12]. Thus, we can make stress engineering efficient for changing the silicon waveguide birefringence. Depending on the specific value of the geometrical birefringence, we can adjust the total modal birefringence to be zero for achieving polarization independent performance of a device.

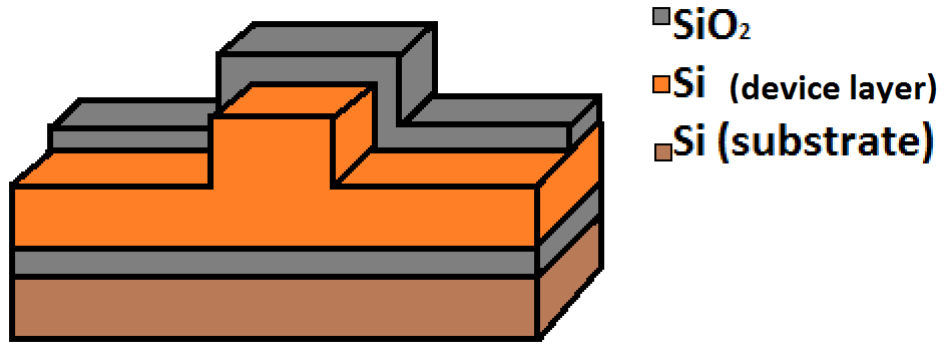


Figure 1.2: Stress induced by the top cladding

However, we have an easier way out, by implementing polarization diversity circuit (see Fig 1.3). This circuit consists of polarization splitters, polarization rotators, and a ring-resonator wavelength filter. The incident light is initially separated into  $TE$  and  $TM$  polarization components by a polarization splitter [6]. The  $TE$ -polarized light from the splitter is directly guided into the ring resonator, which passes only the desired wavelengths. On the other hand,  $TM$ -polarized light from the splitter is guided first to a polarization rotator, where it is converted into  $TE$ -polarized light, and into the ring resonator from the opposite direction to that of the original  $TE$ -polarized light. Since the  $TM$ -polarized light from the splitter has been converted into  $TE$ -polarized light, the ring can also work as a wavelength filter for this light. Thus, in the rest of the circuit, only one polarization needs to be processed.

The basic block diagram representation of the polarization diversity circuit can be seen as depicted in Fig 1.3. Input light that is launched, is finally converted to a

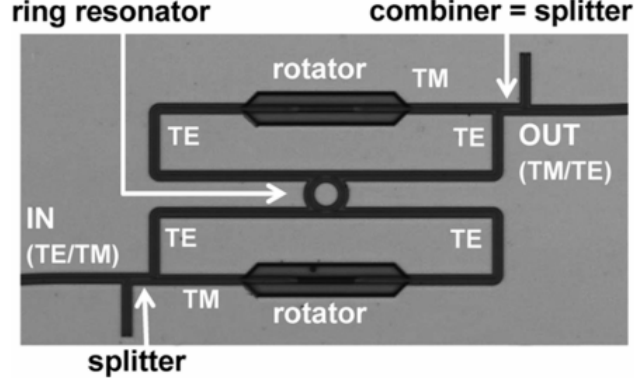


Figure 1.3: A Polarization Diversity Circuit [6]

particular polarization be it  $TE$  or  $TM$  at the output port.

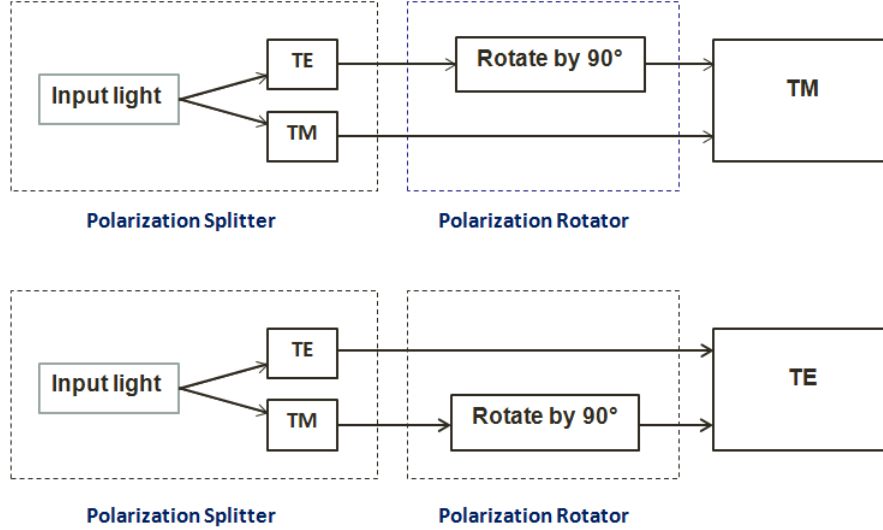


Figure 1.4: Block diagram representation of a PSR

**Directional coupler based :** A PSR can be made by combining an adiabatic taper and an asymmetrical directional coupler [13]. The adiabatic taper structure is designed such that it is single mode at the input end and becomes multimode at the other end. When light propagates along the adiabatic taper structure, the  $TM$  fundamental mode launched at the input is efficiently converted to  $TE_1$  mode at the wide end because of the mode coupling between them. Now we split the  $TE_1$  mode into two  $TE_0$  modes by using an asymmetrical directional coupler that has two adjacent waveguides with different core widths (see Fig 1.5). When the input is  $TE$  polarization, it goes through the taper region unchanged. In directional coupler region, the  $TE_0$  mode is not coupled to the adjacent narrow waveguide because of phase mismatch. The entire length of the device is less

than  $100\ \mu\text{m}$ . This design can be fabricated with a single mask process.

**Y splitter and MMI based :** The PSR is made by combining an adiabatic taper and a Y splitter. (See Fig 1.6) The outputs from the Y splitter are combined together with the help of a  $2\times 2$  MultiMode Interference (MMI) coupler that offers more robustness to the PSR design [14]. In this device, an adiabatically tapered waveguide first converts the  $TM_0$  to the  $TE_1$  mode, while also preserving the  $TE_0$  mode. A  $2\times 2$  MMI coupler, which is well known for its large fabrication tolerance has been utilized for wide bandwidth polarization splitting/combining. It is introduced afterward to effectively couple the  $TE_0$  and  $TE_1$  modes at the end of the  $TM_0 - TE_1$  mode converter to two distinct  $TE_0$  outputs. It can be fabricated in a single lithography and etching step.

## 1.4 Research Objective

Optoelectronic circuits are optimized for a single polarization either  $TE$  or  $TM$ . Therefore, polarization dependence remains a serious obstacle to the efficient functioning of these circuits. So, the primary concern is to overcome the problem of polarization dependence. Many PSR structures have been proposed to eliminate this problem, but each design had its own shortcoming. The stress engineering based polarization independence is difficult to monitor and control. Though waveguide-type polarization splitters and polarization rotators are desired, it is not a simple task to realize them in practice. To rotate the optical axis of a planar waveguide, one has to introduce some specific asymmetrical structures. In case of the directional coupler based PSR, we are able to achieve efficient polarization rotation. However, the directional couplers have low tolerance to fabrication and need high precision in design parameters [15]. These PSR structures usually accompany complicated and difficult fabrication techniques. One has to go for a device that is more robust in terms of fabrication and at the same time offer high efficiency. Therefore, the Y splitter and MMI based PSR seems like a more reliable solution. Though this structure seems very attractive in all respects, not all details of the design parameters are discussed. This gives us more space to explore and work on alternate designs and improve fabrication tolerance and efficiency.

## 1.5 Thesis Organization

This thesis summarizes my understanding of the topic of polarization in photonic wire waveguides. As seen already, Chapter 1 introduces the term polarization and its effects on optical circuits. A few well established designs of PSR have been briefly discussed. Chapter 2 explores the single mode conditions of the waveguides and  $n_{eff}$  for  $TE$  and  $TM$  modes for various widths to study the concept of mode hybridization and also apply the same in designing an adiabatic taper that allows mode conversion from  $TM_0$  to  $TE_1$ . Due to the robustness and fabrication friendliness of the MMI, we chose to delve deeper into the understanding of the PSR structure that has an adiabatic taper followed by a 2x2 MMI in Chapter 3. Working principles and design aspects of the same are also discussed. Tolerance analysis of the Y splitter is studied. Chapter 4 concludes the thesis with the summary and work outcome. Future work that can be done with this design is discussed.

## CHAPTER 2

### Allowed modes in a SOI waveguide

The number of allowed modes in a waveguide depends on its geometrical expanse. By properly designing the dimensions of the waveguide, we can allow only a certain number modes to propagate in it. In this chapter, we will see how the allowed modes in a SOI waveguide are put to use for designing a polarization rotator.

#### 2.1 Single mode condition

In most applications, waveguides are required to support a single mode i.e., lowest order orthogonally polarized  $TE$  and  $TM$  waves, which means only the fundamental mode is allowed to propagate in the waveguide [4].

The single mode region is governed by two distinct conditions, the upper limit being  $TE_1$  and the lower limit being  $TM_0$  due to the differing mode shapes of different polarizations [16].  $TE$  polarization has a more stringent criterion due to the fact that it has two close boundaries where the tangential E field must be met. If the boundaries of the  $TM_0$  and  $TE_1$  cutoffs are rigorously fitted, we can obtain the single mode condition at the wavelength of 1550 nm.

The number of allowed modes in a waveguide depends on its dimensions. As the waveguide dimensions vary, the  $E_x$ ,  $E_y$ ,  $E_z$  and  $H_x$ ,  $H_y$ ,  $H_z$  fields also vary accordingly giving rise to different modes. Depending on the weight factor in each field component, these modes can be classified as  $TE$ ,  $TM$  or mixed modes. (See Fig 1.1) To find out the polarization type of the given mode,  $TE$  fractions (represented as  $\phi$ ) is defined. The  $TE$  polarization fraction  $E_y$  for the propagation along x direction is defined by the following equation:

$$\phi = \frac{\int |E_y|^2 dx dy}{\int (|E_y|^2 + |E_z|^2) dx dy}$$

where the denominator corresponds to  $|E_{parallel}|^2$  since we are considering the polarization of the modes, we only consider the fields parallel to the mode cross section.



This definition helps us in determining the polarization of the mode. If the value of the  $TE$  polarization fraction is greater than 50, we can conclude that the mode is  $TE$ , if the value is less than 50, we say  $TM$  mode. If the value is exactly 50, we cannot precisely conclude what mode it might be. For a height of 250 nm and  $SiO_2$  thickness of 3  $\mu m$  (see Fig 1.1), we vary the width of the silicon photonic wire waveguide, to find out the number of allowed modes. (See Table 2.1) Width of the waveguide is varied to observe how the effective index is increasing as the width of the waveguide is increasing. Also the type of polarization is determined from the value of  $\phi$ . The wavelength used is 1550 nm for the steady state simulation performed using numerical mode solver.

Table 2.1: Exclusive single moded waveguides

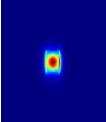
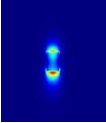
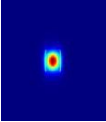
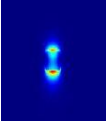
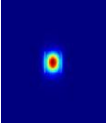
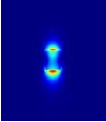
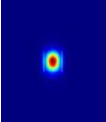
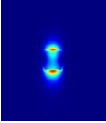
Width(nm)	No of allowed modes	$n_{eff}$ effective indices	Different modes $ E $	$\phi$	Polarization type
400	mode 1	2.2333		96	$TE$
	mode 2	1.7084		7	$TM$
450	mode 1	2.3870		98	$TE$
	mode 2	1.7743		7	$TM$
500	mode 1	2.4957		98	$TE$
	mode 2	1.8314		6	$TM$
550	mode 1	2.5730		99	$TE$
	mode 2	1.8768		6	$TM$

Table 2.2: Waveguide dimensions that allow 3 modes

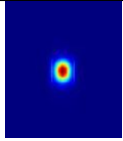
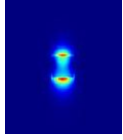
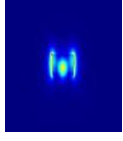
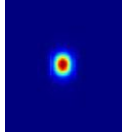
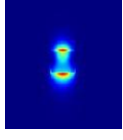
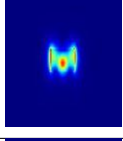
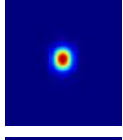
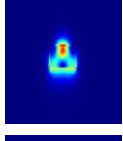
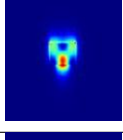
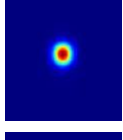
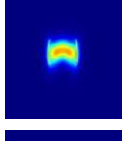
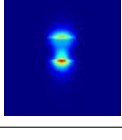
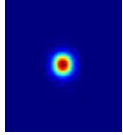
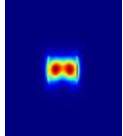
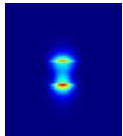
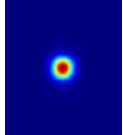
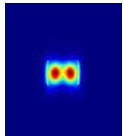
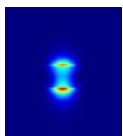
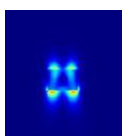
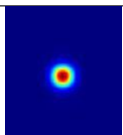
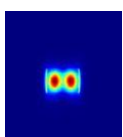
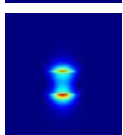
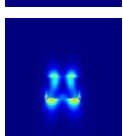
Width(nm)	No of allowed modes	$n_{eff}$ effective indices	Different modes $ E $	$\phi$	Polarization type
600	mode 1	2.6317		99	$TE$
	mode 2	1.9163		6	$TM$
	mode 3	1.5768		81	$TE$
650	mode 1	2.6762		99	$TE$
	mode 2	1.9490		7	$TM$
	mode 3	1.7825		86	$TE$
700	mode 1	2.7116		100	$TE$
	mode 2	1.9912		36	$TM$
	mode 3	1.9445		46	$TM$
750	mode 1	2.7396		100	$TE$
	mode 2	2.1054		93	$TE$
	mode 3	1.9906		6	$TM$

Table 2.3: Waveguide dimensions that allow upto 4 modes with completely evolved  $TE_1$  mode

Width(nm)	No of allowed modes	$n_{eff}$ effective indices	Different modes $ E $	$\phi$	Polarization type
800	mode 1	2.7626		100	$TE$
	mode 2	2.2155		97	$TE$
	mode 3	2.0119		4	$TM$
850	mode 1	2.7814		100	$TE$
	mode 2	2.3036		98	$TE$
	mode 3	2.0286		4	$TM$
	mode 4	1.6128		23	$TM$
900	mode 1	2.7973		100	$TE$
	mode 2	2.3772		98	$TE$
	mode 3	2.0432		4	$TM$
	mode 4	1.6646		23	$TM$

From the tables 2.2 and 2.3, it can be noted that  $TE_1$  mode starts evolving after the width of 700 nm. Also note that the  $n_{eff}$  of  $TM_0$  and  $TE_1$  are almost the same.

## 2.2 $TM_0$ - $TE_1$ hybridization

Plotting the effective index vs the waveguide width for the photonic wire, we obtain the graph shown in Fig 2.1. As seen from the figure, the plots for  $TE_1$  and  $TM_0$  are almost touching each other at around 700 nm. At this critical width of 700 nm (circled in blue),  $TM_0$  and  $TE_1$  modes have almost the same effective index. Therefore, a chance of mode hybridization is highly possible if we design a waveguide appropriately to make this transition happen. A Polarization splitter and rotator can be designed by exploiting this fact.

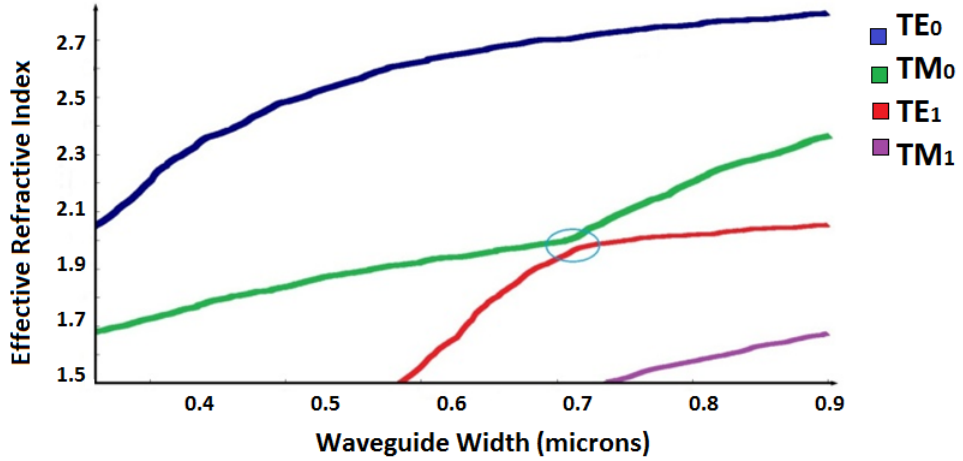


Figure 2.1: Effective Index for different modes as a function of varying width where the blue circle shows the critical point that allows mode conversion between  $TM_0$  and  $TE_1$

## 2.3 Design of an adiabatic taper structure

As seen in table 2.1, the single mode width for the waveguide ranges from 400 nm to 550 nm. And the critical width for the conversion of  $TM_0$  to  $TE_1$  is around 700 nm. For converting the single moded waveguide to a multi moded waveguide, we need to use a taper section whose width varies from single mode region to multi mode region. As mentioned earlier, for efficient  $TM_0 - TE_1$  polarization conversion, a material that

is different from the buffer layer ( $SiO_2$ ) should be applied as top - cladding layer. Generally air is chosen as the top cladding material. Compact devices are generally preferred. Therefore, to decrease the tapering length of the structure, the  $TM_0 - TE_1$  converter is divided into three sections. The first section  $L_1$  is from input single mode silicon waveguide of width 450 nm to width 650 nm. This section does not have a role to play in the mode conversion. Therefore, a short tapering length of 10  $\mu m$  is employed.  $L_1$  helps us in achieving large variation in width ( $\Delta w = 200$  nm) in a short span of length of only 10  $\mu m$ .

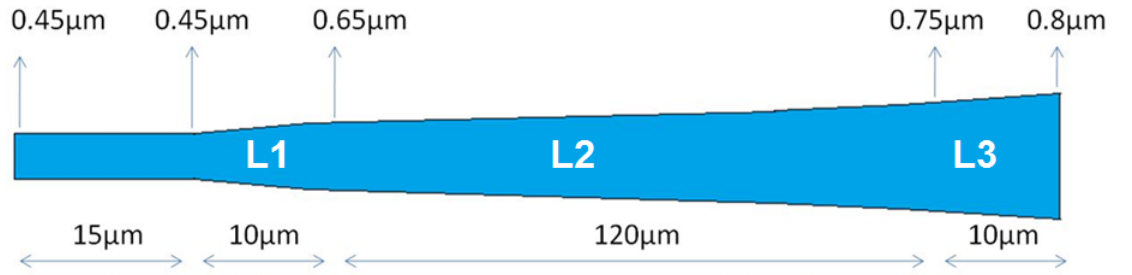


Figure 2.2: Detailed schematic of the taper section with design parameters

Knowing that the  $TM_0$  and  $TE_1$  modes are phase matched around the width of 700 nm, we go for a gradual taper section in the  $L_2$  region. It extends from a width of 650 nm to 750 nm over a span of 120  $\mu m$  tapering length, that can guarantee an efficient  $TM_0 - TE_1$  conversion. The third section  $L_3$  varies from a width of 750 nm to 800 nm over a short length of 10  $\mu m$  to avoid coupling back to  $TM_0$  and any further mode interactions. The design is centered over maintaining  $\Delta\beta$  without disrupting the interaction length to give proper coupling length and also to maintain the phase matching condition. This structure is designed for a SOI platform with the  $SiO_2$  thickness being 3  $\mu m$  and the height of the device layer being 250 nm. Simulation of with these parameters were performed to obtain the following results.

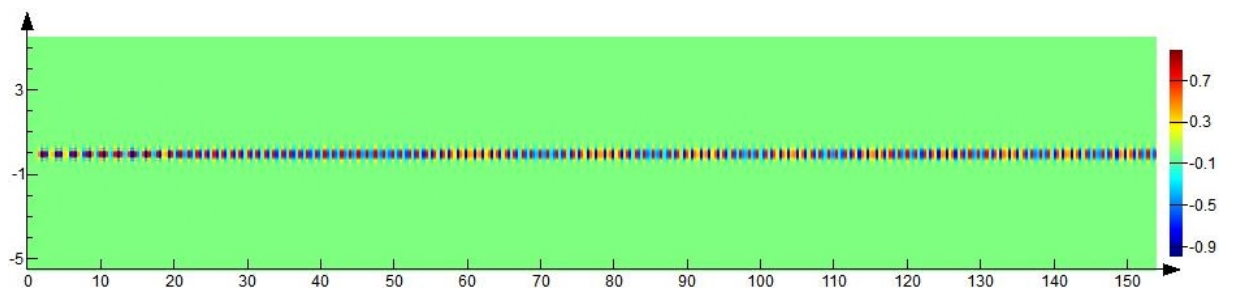


Figure 2.3: FDTD simulated  $E_y$  profile of the light wave when  $TE_0$  is launched

**$TE_0$  input:** When  $TE_0$  mode is launched at the input, it is known that the output mode should also be  $TE_0$ . The simulation seen in Fig 2.3, shows the  $E_y$  profile of the light wave. The Fig 2.5(a) shows that the mode has expanded with the increase in the width, but retained its profile and continues to be  $TE_0$  mode.

**$TM_0$  input:** When  $TM_0$  mode is launched at the input, it is known that the output mode should change to  $TE_1$ . The following simulation as seen in Fig 2.4, shows the magnitude profile of the light wave. The Fig 2.5(b) shows that the mode has changed to  $TE_1$  as the width is increased.

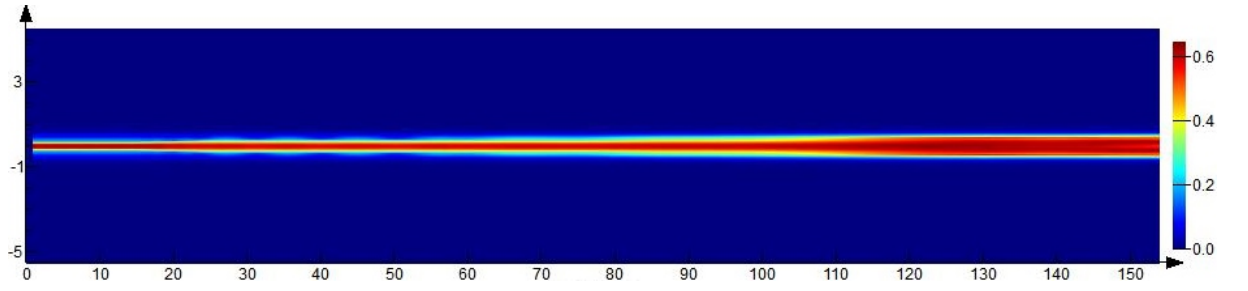


Figure 2.4: FDTD simulated magnitude profile of the light wave when  $TM_0$  is launched

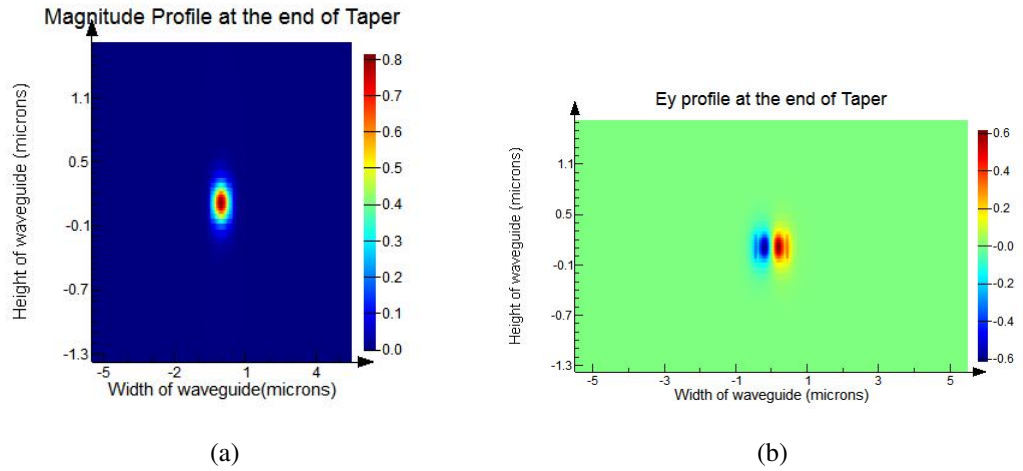


Figure 2.5: (a) FDTD simulated magnitude profile of the output mode at the end of the taper when  $TE_0$  is launched, (b) FDTD simulated  $E_y$  profile of the output mode at the end of the taper when  $TM_0$

## CHAPTER 3

### Design of polarization splitter and rotator

From the previous chapter, note that the mode conversion in the taper has taken place successfully,  $TE_0$  outputs  $TE_0$  and  $TM_0$  outputs  $TE_1$ . Now the next task is to split the  $TE_1$  mode into two  $TE_0$  modes. Directional coupler based splitting of the  $TE_1$  mode requires high precision in fabricating the required coupling length. Therefore, we opt for a Y - splitter at the end of the taper section to split the  $TE_0$  and  $TE_1$  modes.

#### 3.1 Design of Y - Splitter

The Y - splitter is placed at the output end of the taper structure. This splitter has an input base width of 800 nm that splits equally into two arms of width 400 nm each. Loss due to bends is generally high. Bends, asymmetry, will induce some kind of a polarization change to the input light if the structures have sharp bends. Therefore, we prefer gradual bends so that light is still confined to the waveguides without getting radiated as loss and also polarization of the input light is still maintained. The most optimum results are seen if we use the x span of 10  $\mu\text{m}$  and y span of 2  $\mu\text{m}$ .

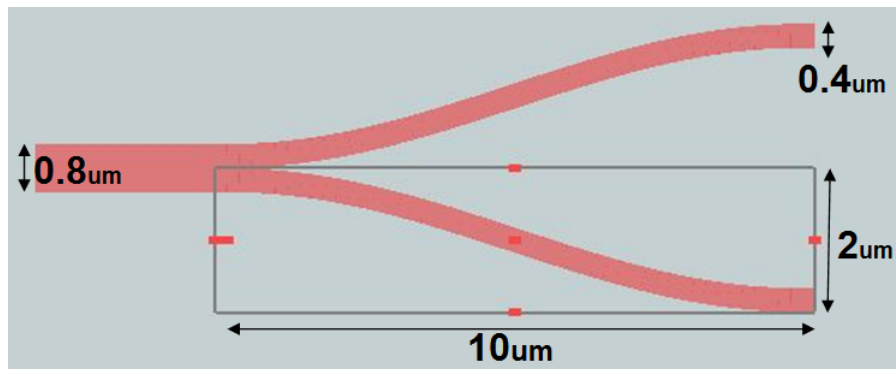


Figure 3.1: Detailed schematic of the Y-Splitter with design parameters

The simulated results for the Y - splitter are shown below

**$TE_0$  input:** When we launch  $TE_0$  mode at the input, we know that the output mode should also be  $TE_0$ . As pointed in Fig 3.2, light in the output ports travel with the

same phase (both mode profiles are red in color) The following simulation shows the  $E_y$  profile of the light wave while propagating through the splitter.

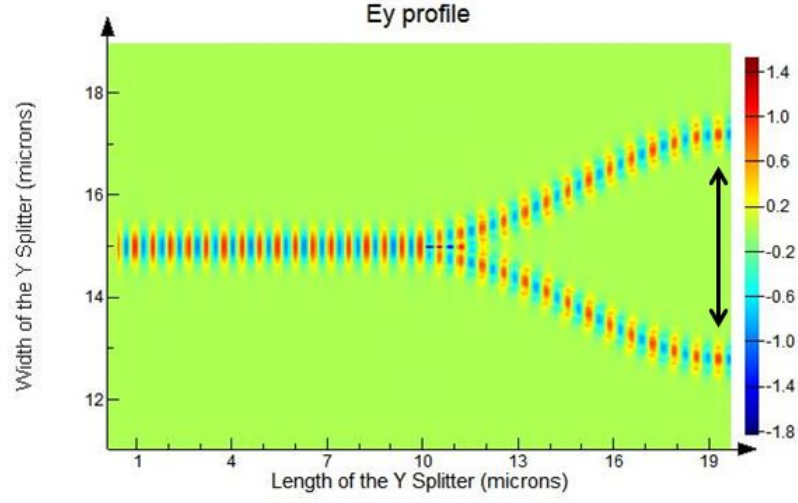


Figure 3.2: FDTD simulated  $E_y$  profile of the light wave when  $TE_0$  is launched

**$TE_1$  input:** When we launch  $TM_0$  mode at the input end of the taper, the output end of the  $TM_0 - TE_1$  converter is split into two arms with each of its output being  $TE_0$ . As pointed in Fig 3.3, light in the output ports travel with a phase difference of  $\pi$  (upper arm output profile is blue, where as lower arm is red). The following simulation shows the  $E_y$  profile of the light wave and the output mode at the end of one of the arms of the Y - splitter.

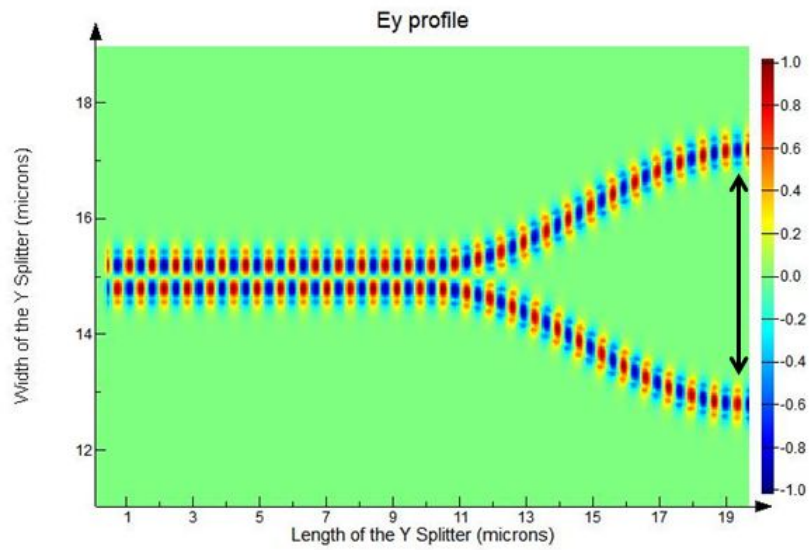


Figure 3.3: FDTD simulated  $E_y$  profile of the light wave when  $TE_1$  is launched

The output mode at the end of one of the arms of the Y - splitter for any input  $TE_0$  or  $TM_0$  is the same as shown below in Fig 3.4.



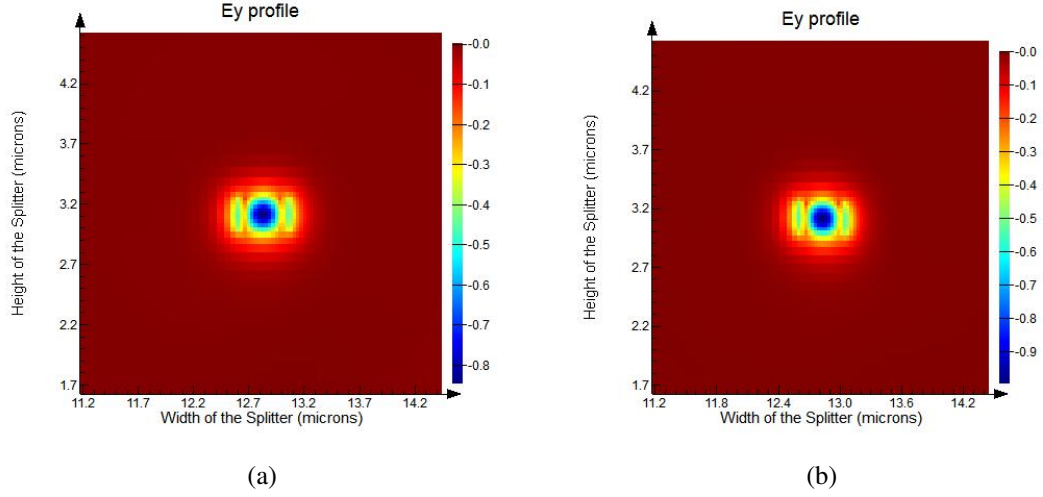


Figure 3.4: (a) Simulated  $E_y$  mode profile of the light wave at the end of the splitter, when  $TE_0$ , (b) Simulated  $E_y$  mode profile of the light wave at the end of the splitter, when or  $TM_0$  is launched

### 3.2 Combining the adiabatic taper and the Y - splitter

After combining the taper section with the Y - splitter, we obtain the required polarization splitter and rotator. The output in both the arms of the Y - splitter is  $TE_0$ . The following simulations show the propagation of light through this structure.

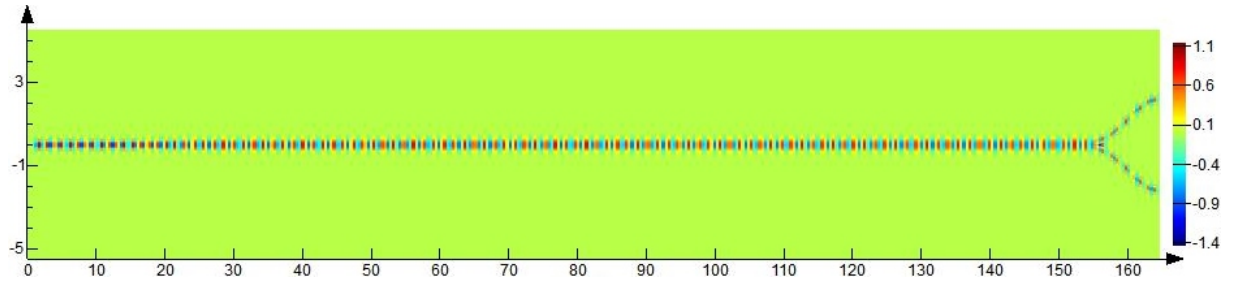


Figure 3.5: Simulated  $E_y$  profile of the light wave when  $TE_0$  is launched

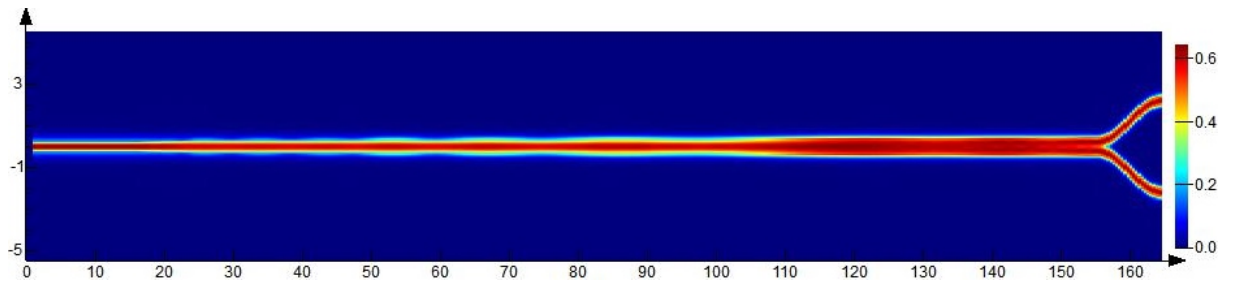


Figure 3.6: Simulated magnitude profile of the light wave when  $TM_0$  is launched

### 3.3 MMI Design

Though the polarization splitter and rotator has been designed, as seen in Fig 3.5 and Fig 3.6, the total output does not exit from the same port. There are two arms of the Y - splitter which output  $TE_0$  in each arm. Now the next step to take is to combine both the arms of the Y - splitter and output the total light from a single output port. The best and robust structure that we can use for combining light is by using an MMI coupler.

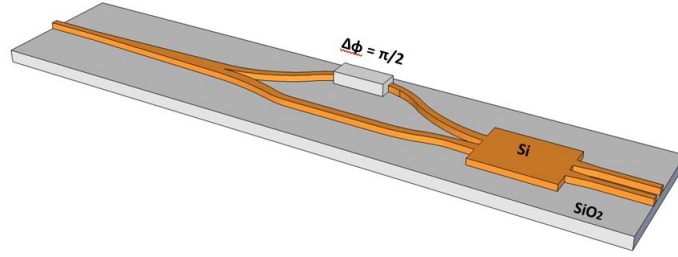


Figure 3.7: 3D view of the PSR structure

A 2x2 MMI coupler, which is well known for its large fabrication tolerance[17], is introduced to effectively couple the  $TE_0$  and  $TE_1$  modes at the end of the  $TM_0 - TE_1$  mode converter to two distinct  $TE_0$  outputs. When the input launched is  $TE_0$ , the Y - splitter splits it into two  $TE_0$  beams with the same phase difference. Therefore at the MMI input, the two beams will have a phase difference of 90 degrees. Light will output from the lower arm with a little crosstalk in the upper arm. On the other hand, when the input launched is  $TM_0$ , the Y - splitter, the light converted to  $TE_1$  mode will split into two  $TE_0$  beams with 180 degree phase difference. Therefore at the MMI input, the two beams will have a phase difference -90 degrees and light will output from the upper arm with crosstalk in the lower arm.

The 2x2 MMI is designed to be of the symmetric type. We can excite the MMI at either  $\frac{w}{4}$  or  $\frac{w}{6}$ . If we employ the  $\frac{w}{4}$  excitation, the length needed for the MMI is very long. Moreover, efficiency of the MMI for 90 degree phase difference is lower compared to  $\frac{w}{6}$  excitation. A restricted type MMI (excited at  $\frac{w}{6}$ ), could efficiently decrease the length of the MMI. However, at the same time we have to increase the width of the MMI in order to sufficiently separate the two output waveguides.

Going for a restricted type MMI, values like  $3 \mu\text{m}$ ,  $3.6 \mu\text{m}$ ,  $4.2 \mu\text{m}$  can be taken for the width, so that  $\frac{w}{6}$  is not an irrational number. For the two input ports, we choose a tapering length of  $10 \mu\text{m}$  starting from  $400 \text{ nm}$  to  $1000 \text{ nm}$ . We simulate the structure

with an open end to precisely locate the required self-imaging points[18]. Thus, we place our output ports accordingly.

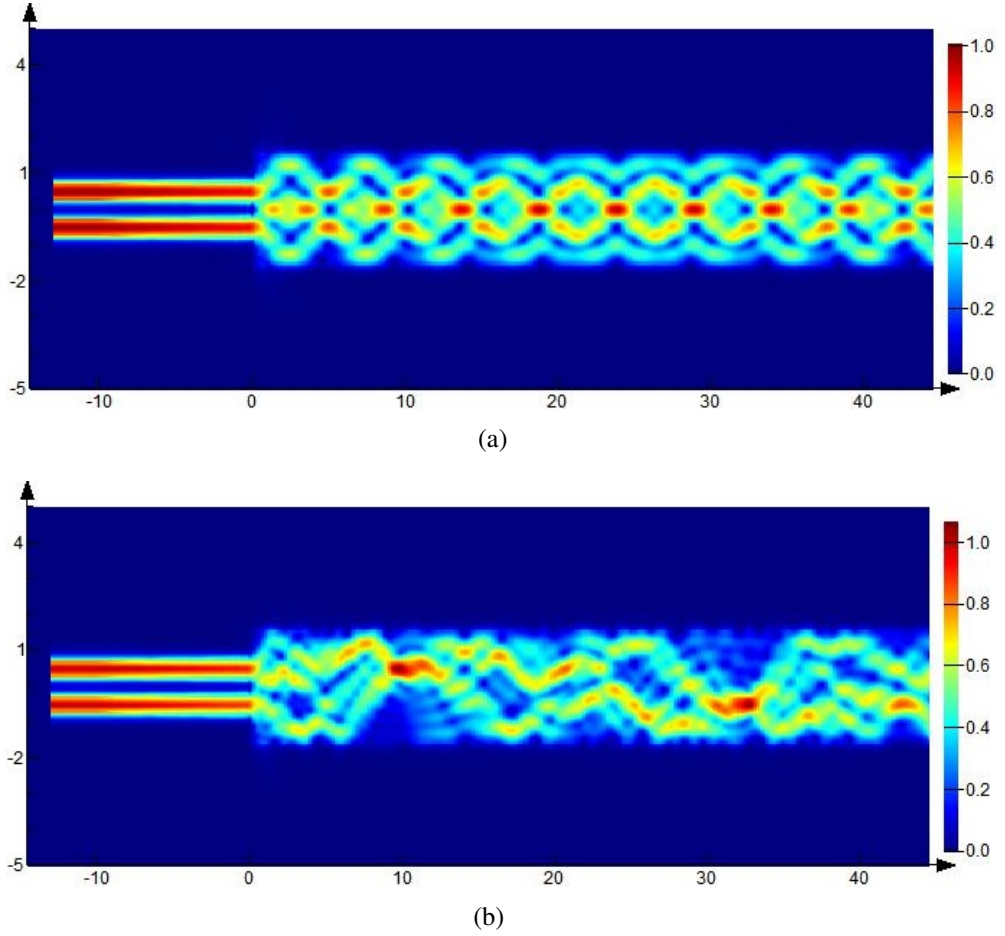
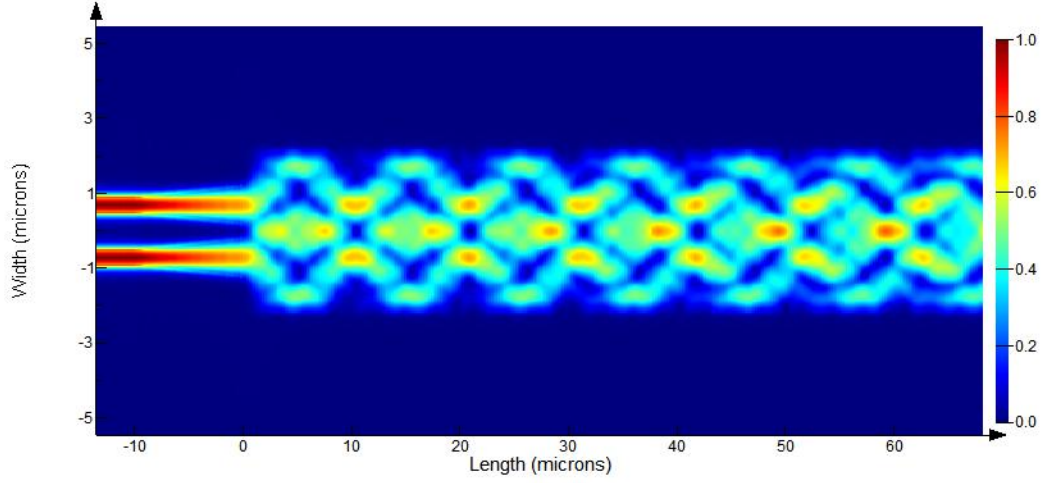


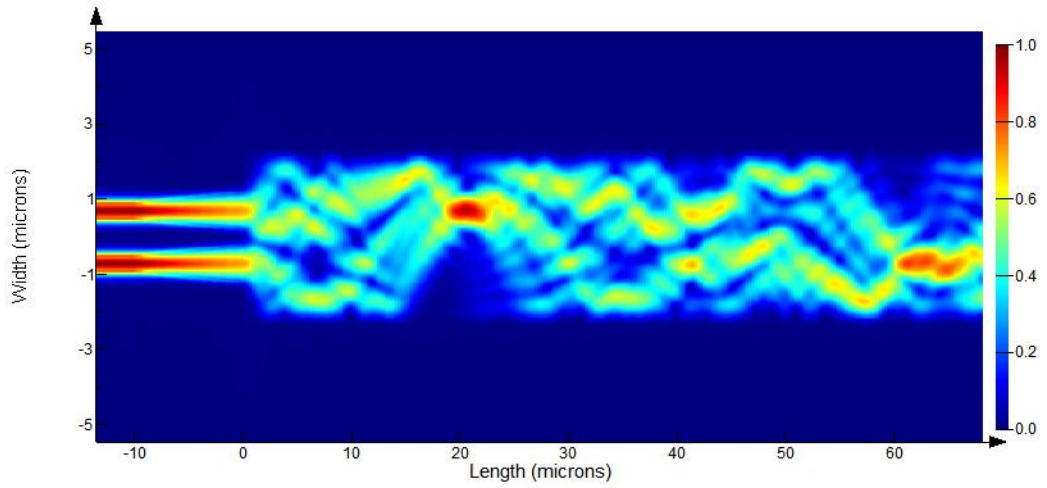
Figure 3.8: (a)Simulation of a  $3 \mu\text{m}$  width MMI structure with 0 degree phase difference between the two sources, (b)Simulation of a  $3 \mu\text{m}$  width MMI structure with 90 degree phase difference between the two sources

From Fig 3.8(a), it can be noted that all the modes are not completely evolved. Two images cannot be identified precisely as the modes are little dispersed. Therefore higher widths are preferred. Simulations have been performed for width like  $3.6 \mu\text{m}$ ,  $4.2 \mu\text{m}$  and  $4.8 \mu\text{m}$ . The width of  $3.6 \mu\text{m}$  also does not let all the modes evolve and precisely identifying two images would still be difficult. Though the width of  $4.8 \mu\text{m}$  lets the modes evolve and also allows precise identification of two images, the length of the structure becomes very large. Therefore the optimum width of  $4.2 \mu\text{m}$  is chosen as it allows precise identification of two images, also the length of the structure is reasonable.

The Fig 3.9(a) shows the light propagation when the phase difference between the two sources is 0 degrees. Fig 3.9(b) is when the phase difference is 90 degrees. simulation is performed with an open end launching  $TE_0$  at both the inputs.



(a)



(b)

Figure 3.9: (a)Simulation of a 4.2  $\mu\text{m}$  width MMI structure with 0 degree phase difference between the two sources, (b)Simulation of a 4.2  $\mu\text{m}$  width MMI structure with 90 degree phase difference between the two sources

We see that at approximately 20.5  $\mu\text{m}$  we can see that the images for both the simulations coincide. Therefore we place the output ports at that length to obtain maximum efficiency. The final design parameters for the MMI structure can be seen in the following Fig 3.10

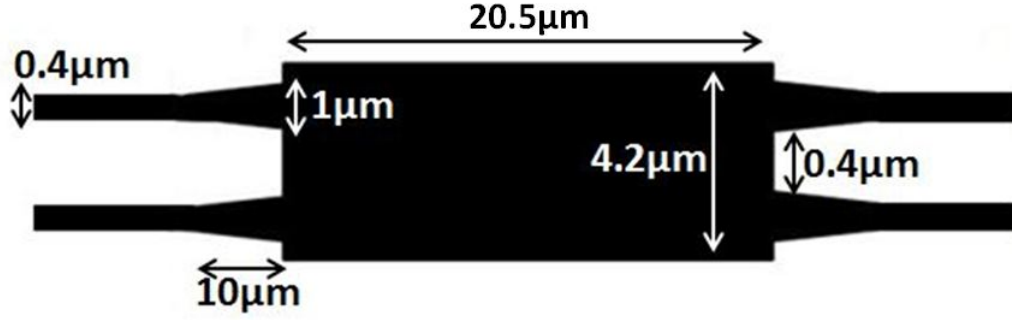


Figure 3.10: MMI design parameters

### 3.4 90 degree Phase shift

The two arms of the Y - splitter are designed to have a phase difference of 90 degrees. To employ the same we can use several methods to obtain the 90-degree phase shift. Adding a suitable extra path length in one of the arms will give us a phase of 90 degrees. However, it would be difficult to implement in practice as the extra path length has to be given in the bend regions by maintaining symmetry so that polarization rotation does not take place.

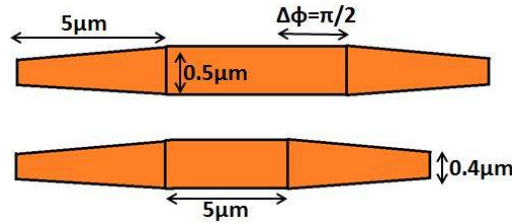


Figure 3.11: Schematic of the 90 degree phase difference using width variation

We can implement another method by playing around with the width of the arms to obtain the 90-degree phase shift. The  $n_{eff}$  is a function of width of the waveguide. Exploiting this fact, we can increase the width of the arms of Y splitter from 400 nm to some higher value and adjust the length accordingly to obtain the 90-degree phase difference.

We know that  $\beta(\Delta L) = m\frac{\pi}{2}$

From table we know the values of

$$n_{eff} \text{ for } 400\text{nm} = 2.233371$$

$$n_{eff} \text{ for } 450\text{nm} = 2.387055$$

$$n_{eff} \text{ for } 500\text{nm} = 2.495724$$

$$2L\pi \frac{(n_{eff450} - n_{eff400})}{\lambda} = m\frac{\pi}{2}$$

Solving for the value of  $L$  we obtain the extra path length needed to attain the 90 degree phase shift. The following is the simulation result when we combine the Y splitter, the 90-degree phase difference and the MMI

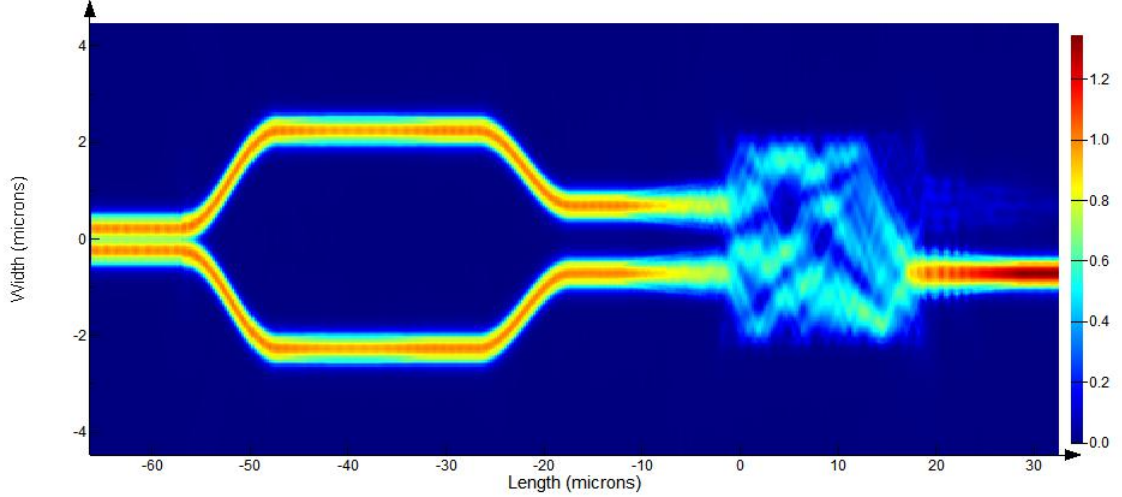


Figure 3.12: Simulated structure of device using width variation for 90 degree phase difference

We must also keep in mind that the taper section used for increasing the width from 400 nm, might not be adiabatic if the change is too abrupt. The taper region must be long enough to not excite higher order modes. Also we need to keep the device as compact as possible, therefore we need to choose wisely.

If we opt for 400 nm to 500 nm width change, the possible values of  $L$  for different values of odd integer  $m$  are  $1.477\mu\text{m}$ ,  $4.431\mu\text{m}$ ,  $7.385\mu\text{m}$  and so on.

If we opt for 400 nm to 450 nm width change, the possible values of  $L$  for different values of odd integer  $m$  are  $2.521\mu\text{m}$ ,  $7.563\mu\text{m}$ ,  $12.605\mu\text{m}$  and so on.

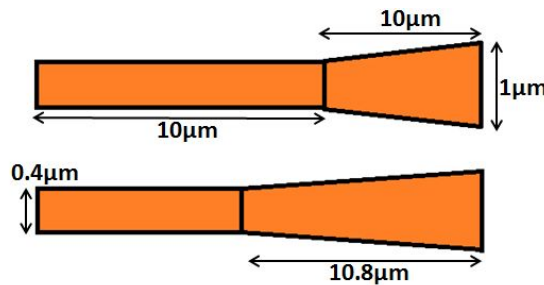


Figure 3.13: Schematic of the 90 degree phase difference using taper length variation

We can also implement using another method by playing around with one of the tapering lengths of the MMI input ports to obtain the 90-degree phase shift (see Fig



3.15). Retaining the same old parameters for the lower input port, we vary the length of the upper port to obtain the phase difference.

After simulations, we see that in the upper port, the original tapering length of  $10\ \mu\text{m}$  starting from  $400\ \text{nm}$  to  $1000\ \text{nm}$  is increased to  $10.8\ \mu\text{m}$  to obtain the required 90-degree phase difference.

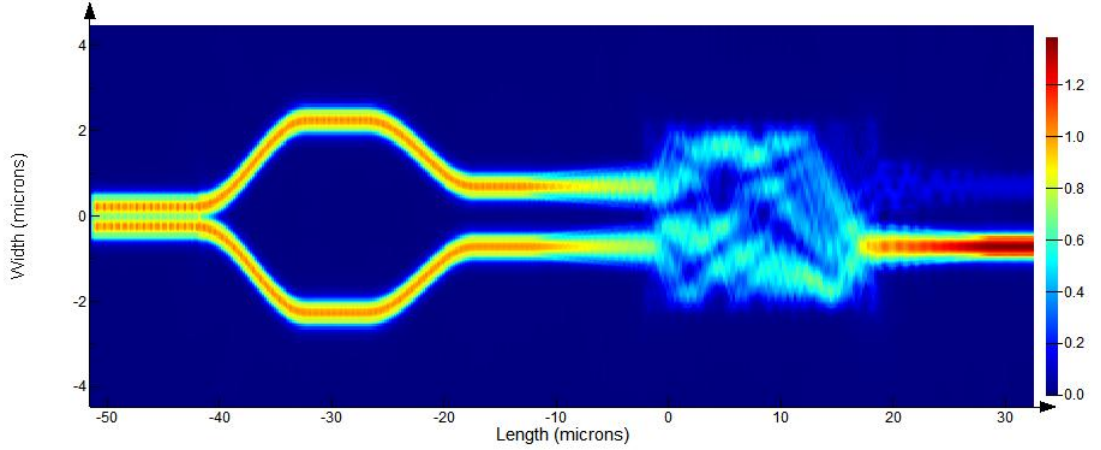


Figure 3.14: Simulated structure of device using taper length variation for 90 degree phase difference

We see that both the methods give us the same efficiency but the second method of varying the taper length is more compact by offering the same results with an advantage of reducing the length by  $10\ \mu\text{m}$ .

### 3.5 Principle and working of the PSR

When the upper cladding is same as the buffer layer ( $\text{SiO}_2$ ), the SOI nanowire is vertically symmetrical and therefore the modes in this waveguide are purely polarized. If on the other hand, the upper cladding index is not equal to that of the buffer layer ( $\text{SiO}_2$ ), the mode properties become more complicated and one cannot distinguish the polarization of some eigenmodes because of the mode hybridization. Such mode hybridization will introduce a mode conversion when light propagates along an adiabatic taper structure. Using this principle we can design taper structure of varying core width such that mode conversion takes place between the  $TM_0$  fundamental mode and the first higher order mode of  $TE$  polarization.

The polarization splitter and rotator consists of a taper that is single moded at the input end while it becomes multimode at the other end. When light propagates along the taper structure, the  $TM_0$  fundamental mode launched at the narrow end is converted to the first higher order  $TE$  mode at the wide end because of the mode coupling between them. On the other hand, the input  $TE$  polarization keeps the same polarization state when it goes through the taper structure.

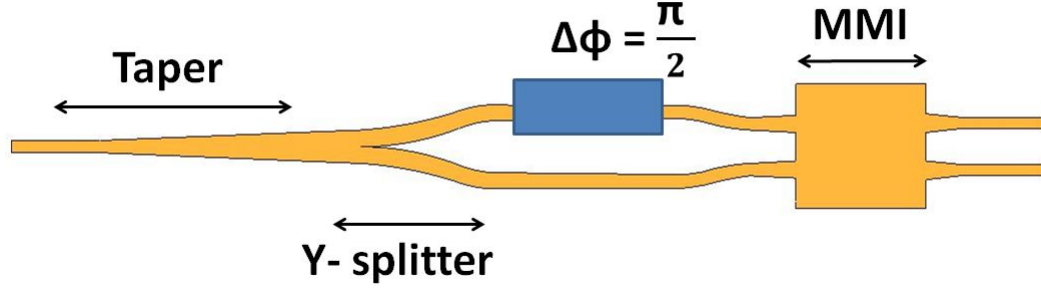


Figure 3.15: Topview of PSR with all the components

The other end of the taper structure diverges as a Y splitter. Before being injected into the 2x2 MMI, an extra phase difference of 90 degrees is introduced between the two beams. In case of  $TE_0$  input, the mode will be preserved during the adiabatic taper and split into two  $TE_0$  beams with the same phase. Thus, at the MMI input, the two beams will have a 90 degree phase difference. By appropriately designing the MMI, light will output from the upper arm on the  $TE_0$  mode with little crosstalk in the lower arm. On the other hand, in case of  $TM_0$  input, the light is converted to the  $TE_1$  mode during the adiabatic tapering and split into two  $TE_0$  beams with a  $\pi$  phase shift. Thus at the MMI input, the two beams will have a -90 degree phase difference, and light will consequently output from the lower arm on the  $TE_0$  mode with little crosstalk in the upper arm.

### 3.6 Tolerance analysis of Y - Splitter

Though we get very good results with the Y- splitter of the given dimensions, it is very critical to fabricate the same. The minimum feature size of the device is the inner corner of the Y-splitter.

To make the device fabrication friendly, we can add a taper region of length  $10 \mu\text{m}$



Gap(nm)	Transmittance of $TE_0$	Total Transmittance	Transmittance of $TM_0$	Total Transmittance
0	0.4815	0.9630	0.5000	1.0000
50	0.4671	0.9342	0.4994	0.9988
100	0.4200	0.8400	0.4969	0.9938

Table 3.1: Variation of efficiency with Y-spiltter gap.

with a width varying from 800 nm to 900 nm and introduce a gap of 100 nm between the two arms of the Y - splitter and keep the rest of the device structure same. In this way, we can make fabrication less complicated, but we are also losing on efficiency for ( $TE_0$ ) input

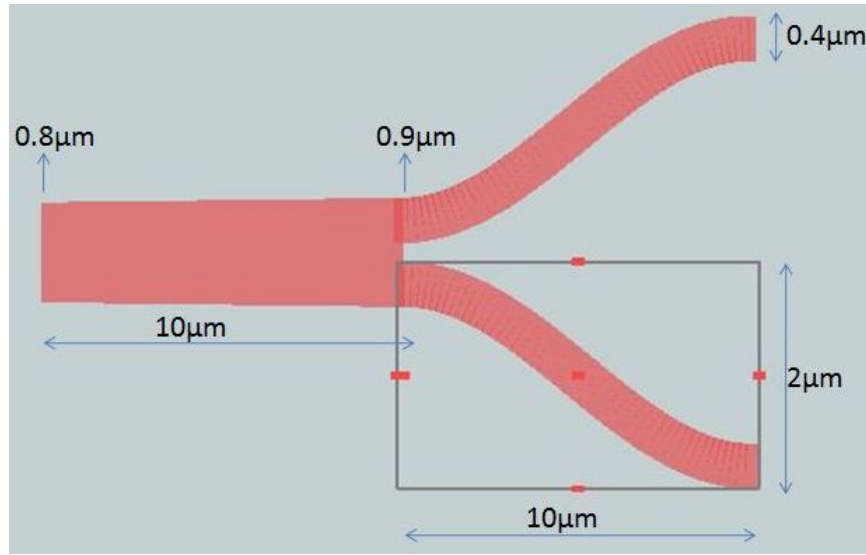


Figure 3.16: Y - splitter with a gap of 100nm

In case of  $TE_0$ , we know that the mode is more confined to the center of the waveguide. When we introduce a gap of 100 nm in the center, some of the light is leaked out here, giving us lesser efficiency.

However, when the input launched is  $TM_0$ , the efficiency of this structure is still very high. In the taper region, the  $TM_0$  mode is eventually converted into  $TE_1$  mode. From the mode profile of  $TE_1$ , we can see that there are two lobes that are concentrated more towards the edges of the waveguide. Therefore there is no much loss seen even if we introduce a gap of 100 nm in the Y splitter.

### 3.7 Complete structure

Combining the taper region with the MMI maintaining the 90-degree phase difference, we obtain the complete structure of the Polarization splitter and rotator. The total device length can vary between  $220\text{ }\mu\text{m}$  to  $250\text{ }\mu\text{m}$  based on our requirements of fabrication friendliness or higher efficiency. The box height used for the structure is  $3\text{ }\mu\text{m}$ . The highest attainable efficiency for the device (with  $100\text{ nm}$  gap) when  $TM_0$  is launched is 98.92 percent. Whereas the lowest attainable efficiency for the device (with  $100\text{ nm}$  gap) when  $TE_0$  is launched is 82.67 percent.

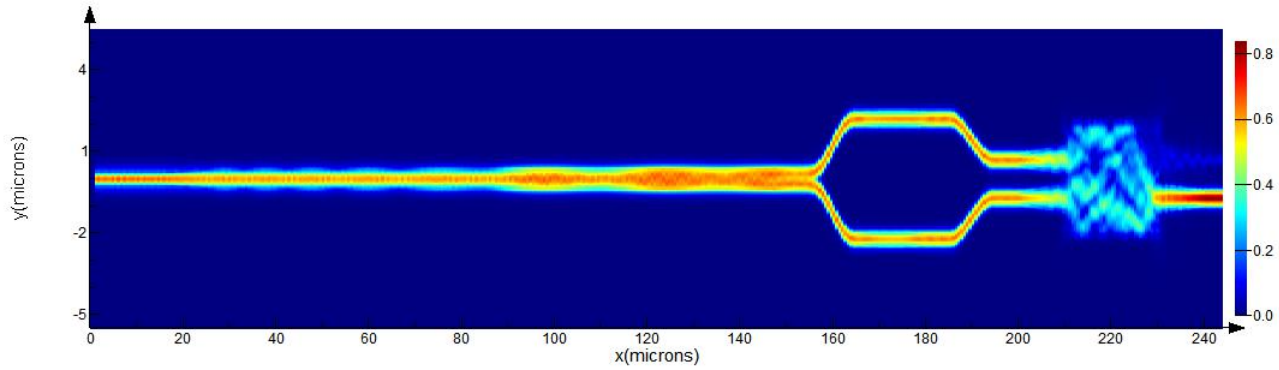


Figure 3.17: Simulation of the complete PSR structure when  $TM_0$  is launched

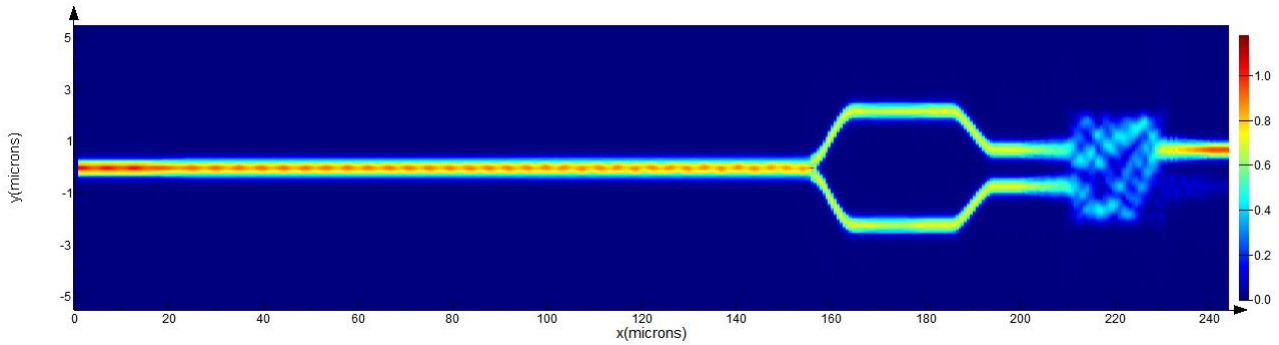


Figure 3.18: Simulation of the complete PSR structure when  $TE_0$  is launched

# CHAPTER 4

## Summary and future work

### 4.1 Summary

A polarization splitter and rotator was designed and optimized to get  $TE_0$  as the output for both  $TE_0$  and  $TM_0$  inputs. Alternate structures and design parameters for the PSR are discussed. Alternate designs that can be used instead of extra path length for achieving a 90 degree phase difference are discussed. A 2x2 MMI is optimized to achieve maximum efficiency for 90 degree phase difference at the output. All the simulations for the optimization of the design are done using the Lumerical FDTD simulation tool. This PSR structure is simulated for SOI platform with silicon thickness being 250 nm and buried  $SiO_2$  being 3  $\mu\text{m}$ . The total device length can vary between 220  $\mu\text{m}$  and 250  $\mu\text{m}$  based on our requirements of fabrication friendliness or higher efficiency. Tolerance analysis for the Y - splitter was done to understand the fabrication and efficiency limits.

### 4.2 Future work

The design and optimized structure now needs to be fabricated on the SOI platform using a single step E beam lithography. This fabricated structure, then needs to be characterized and tested. The device structure can be further improved by designing a better splitter than the already existing Y - splitter to make it more fabrication friendly. The minimum feature size of the device should be increased (for low loss, it had 0 gap) to make it more tolerant to fabrication. The number of taper sections can be reduced to get a more smooth structure. The device can be made more compact.

## REFERENCES

- [1] Micro e bulletin. 3, 2009.
- [2] Pieter Dumon, Wim Bogaerts, Vincent Wiaux, Johan Wouters, Stephan Beckx, Joris Van Campenhout, Dirk Taillaert, Bert Luyssaert, Peter Bienstman, Dries Van Thourhout, et al. Low-loss soi photonic wires and ring resonators fabricated with deep uv lithography. *IEEE Photonics Technology Letters*, 16(5):1328–1330, 2004.
- [3] Rupesh Kumar Navalakhe, Nandita DasGupta, and Bijoy Krishna Das. Fabrication and characterization of straight and compact s-bend optical waveguides on a silicon-on-insulator platform. *Applied Optics*, 48(31):G125–G130, 2009.
- [4] B Eng. *W infinie Ning Ye*. PhD thesis, Carleton University, 2006.
- [5] Limin Tong, Jingyi Lou, and Eric Mazur. Single-mode guiding properties of subwavelength-diameter silica and silicon wire waveguides. *Optics Express*, 12(6):1025–1035, 2004.
- [6] Koji Yamada. Silicon photonic wire waveguides: fundamentals and applications. In *Silicon Photonics II*, pages 1–29. Springer, 2011.
- [7] Dan-Xia Xu, Siegfried Janz, and Pavel Cheben. Design of polarization-insensitive ring resonators in silicon-on-insulator using mmi couplers and cladding stress engineering. *Photonics Technology Letters, IEEE*, 18(2):343–345, 2006.
- [8] PR Graves, G Hua, S Myhra, and JG Thompson. The raman modes of the aurivillius phases: temperature and polarization dependence. *Journal of Solid State Chemistry*, 114(1):112–122, 1995.
- [9] Eyal Lichtman. Limitations imposed by polarization-dependent gain and loss on all-optical ultralong communication systems. *Journal of Lightwave Technology*, 13(5):906–913, 1995.
- [10] Tymon Barwicz, Michael R Watts, Miloš A Popović, Peter T Rakich, Luciano Socci, Franz X Kärtner, Erich P Ippen, and Henry I Smith. Polarization-transparent microphotonic devices in the strong confinement limit. *Nature Photonics*, 1(1):57–60, 2007.
- [11] Dan-Xia Xu, André Delâge, Siegfried Janz, and Pavel Cheben. Broadband polarization compensation in silicon-on-insulator components using cladding stress engineering. In *Photonics North 2008*, pages 70991O–70991O. International Society for Optics and Photonics, 2008.
- [12] Lorenzo Pavesi and David J Lockwood. *Silicon Photonics*, volume 1. Springer, 2004.

- [13] Daoxin Dai and John E Bowers. Novel concept for ultracompact polarization splitter-rotator based on silicon nanowires. *Optics Express*, 19(11):10940–10949, 2011.
- [14] Yunhong Ding, Haiyan Ou, and Christophe Peucheret. Wideband polarization splitter and rotator with large fabrication tolerance and simple fabrication process. *Optics Letters*, 38(8):1227–1229, 2013.
- [15] M Rajarajan, BMA Rahman, and KTV Grattan. A rigorous comparison of the performance of directional couplers with multimode interference devices. *Journal of Lightwave Technology*, 17(2):243–248, 1999.
- [16] Soon T Lim, Ching E Png, Eng A Ong, and Yong L Ang. Single mode, polarization-independent submicron silicon waveguides based on geometrical adjustments. *Optics Express*, 15(18):11061–11072, 2007.
- [17] Lucas B Soldano and Erik CM Pennings. Optical multi-mode interference devices based on self-imaging: principles and applications. *Journal of Lightwave Technology*, 13(4):615–627, 1995.
- [18] M Bachmann, PA Besse, and Hans Melchior. General self-imaging properties in  $n \times n$  multimode interference couplers including phase relations. *Applied Optics*, 33(18):3905–3911, 1994.